

The ESO Nearby Abell Cluster Survey¹
XII. The mass and mass-to-light-ratio profiles of rich clusters

Peter Katgert

Sterrewacht Leiden, Postbus 9513, Niels Bohrweg 2, 2300 RA Leiden, The Netherlands

katgert@strw.leidenuniv.nl

Andrea Biviano

INAF/Osservatorio Astronomico di Trieste, Via Tiepolo 11, I-34131 Trieste, Italy

biviano@ts.astro.it

and

Alain Mazure

*OAMP/Laboratoire Astrophysique de Marseille, Traverse du Siphon, Les Trois Lucs, BP 8,
F-13376 Marseille Cedex, France*

alain.mazure@oamp.fr

ABSTRACT

We determine the mass profile of an ensemble cluster built from 3056 galaxies in 59 nearby clusters observed in the ESO Nearby Abell Cluster Survey. The mass profile is derived from the distribution and kinematics of the Early-type (elliptical and S0) galaxies only, with projected distances from the centers of their clusters $\leq 1.5 r_{200}$. These galaxies are most likely to meet the conditions for the application of the Jeans equation, since they are the oldest cluster population, and are thus quite likely to be in dynamical equilibrium with the cluster potential. In addition, the assumption that the Early-type galaxies have isotropic orbits is supported by the shape of their velocity distribution. For galaxies of other types (the brightest ellipticals with $M_R \leq -22 + 5 \log h$, and the early and late spirals) these assumptions are much less likely to be satisfied. For the determination of the mass profile we also exclude Early-type galaxies in subclusters. Application of the Jeans equation yields a *non-parametric estimate* of the cumulative mass profile $M(< r)$, which has a logarithmic slope of -2.4 ± 0.4 in the density profile at r_{200} (approximately the virial radius). We compare our result with several analytical models from the literature, and we estimate their best-fit parameters from a comparison of observed and predicted velocity-dispersion profiles. We obtain acceptable solutions for all models (NFW, Moore et al. 1999, softened isothermal sphere, and Burkert 1995). Our data do not provide compelling evidence for the existence

of a core; as a matter of fact, the best-fitting core models have core-radii well below $100 h^{-1}$ kpc. The upper limit we put on the size of the core-radius provides a constraint for the scattering cross-section of dark matter particles. The total-mass density appears to be traced remarkably well by the luminosity density of the Early-type galaxies. On the contrary, the luminosity density of the brightest ellipticals increases faster towards the center than the mass density, while the luminosity density profiles of the early and late spirals are somewhat flatter than the mass density profile.

Subject headings: Galaxies: clusters: general – Galaxies: kinematics and dynamics – Cosmology: observations

1. Introduction

Many attempts have been made to determine the amount and distribution of dark matter in clusters, since Zwicky (1933, 1937) and Smith (1936) concluded that the mass implied by the sum of the luminosities of the galaxies falls short of the total mass by as much as a factor of 10. In recent years, cosmological simulations have shown that dark matter halos have a universal density profile (Navarro, Frenk, & White 1996, 1997; NFW hereafter), but its precise form is still debated (Moore et al. 1999, M99 hereafter), while the ‘universality’ of the mass density profile has also been questioned (Jing & Suto 2000; Thomas et al. 2001; Ricotti 2002). The issue is critical, since knowledge of the total mass (visible and dark, baryonic and non-baryonic) of clusters, and of its distribution (also in relation to the light distribution), gives important clues about the formation process of the clusters (e.g. Crone, Evrard, & Richstone 1994; Jing et al. 1995), and of the galaxies in them (e.g. Mamon 2000), as well as on the nature of dark matter (see, e.g., Natarajan et al. 2002a).

The dark matter can be ‘weighed’ and ‘imaged’ in three ways. First, the gravitational lensing of distant objects yields an estimate of the projected mass distribution in the cluster (see e.g. Tyson, Wenk, & Valdes 1990; Squires et al. 1996). The mass density profile can subsequently be derived assuming the geometry of the cluster. Lensing mostly works for clusters at intermediate and large distances since the lensing equation is unfavourable for nearby clusters, and only few nearby cluster lenses are known (see e.g. Campusano, Kneib, & Hardy 1998). Some results from gravitational lensing observations are consistent with the NFW profile (e.g. Athreya et al. 2002; Clowe & Schneider 2001), while others favour flatter mass density profiles, such as the isothermal sphere (see Fischer & Tyson 1997; Sand, Treu, & Ellis 2002; Shapiro & Iliev 2000; Taylor et al. 1998).

¹Based on observations collected at the European Southern Observatory (La Silla, Chile)
<http://www.astrsp-mrs.fr/www/enacs.html>

A second method uses the distribution of the hot, X-ray emitting, gas in the cluster potential, and the radial variation of the temperature of the gas (see e.g. Hughes 1989; Ettori, De Grandi, & Molendi 2002). Recently, temperature maps have become available for a sizable number of clusters (see e.g. Markevitch et al. 1998; Irwin & Bregman 2000; De Grandi & Molendi 2002). However, the uncertainties in the X-ray temperature profiles are still substantial (see e.g. Irwin, Bregman, & Evrard 1999; Kikuchi et al. 1999), with corresponding uncertainties in the total mass and the mass profile. Moreover, X-ray observations in general sample only the inner cluster regions, even with the new class of X-ray satellites (see, e.g., Pratt & Arnaud 2002). Cooling can also play a rôle, although it is probably not dominant (Suginohara & Ostriker 1998). Most recent results from X-ray observations indicate consistency with the NFW or the M99 profile (e.g. Allen, Ettori, & Fabian 2001; Allen, Schmidt, & Fabian 2002; Markevitch et al. 1999; Pratt & Arnaud 2002; Tamura et al. 2000), but a flatter mass density profile like that of the isothermal sphere seems to be preferred in some clusters (Arieli & Rephaeli 2003; Ettori et al. 2002). Generally, the distribution of the the X-ray emitting gas is found to be flatter than that of the total cluster mass (e.g. Allen et al. 2001, 2002; Markevitch & Vikhlinin 1997; Nevalainen, Markevitch, & Forman 1999, Pratt & Arnaud 2002).

The third, and most traditional way to probe the dark matter content and its distribution in clusters is through the kinematics and spatial distribution of 'tracer particles' moving in the cluster potential. The virial theorem applied to the galaxy population gives an estimate of the total mass but, since the data in general comprise only the central part of a cluster, projection effects and possible anisotropy of the velocity distribution must be taken into account for an accurate estimate (see e.g. Heisler, Tremaine, & Bahcall 1985; The & White 1986). In addition, the virial theorem assumes that mass follows light and if this assumption is not justified that can have a large effect on a cluster mass estimate (see, e.g., Merritt 1987).

Recently, Diaferio & Geller (1997; see also Diaferio 1999) used the caustics in the plane of line-of-sight velocities vs. clustercentric distances to estimate the amplitude of the velocity field in the infall region. This yields an estimate of the escape velocity at several distances, and thus of the mass distribution. This method has the advantage of being free of the assumption of dynamical equilibrium, and hence can be (and has been) used to constrain the cluster mass distribution well beyond the virialization region (Geller, Diaferio, & Kurtz 1999; Reisenegger et al. 2000; Rines et al. 2000, 2001, 2002; Biviano & Girardi 2003). However, systematic uncertainties limit the accuracy in the mass determination to $\sim 50\%$ (Diaferio 1999). Results obtained with this method indicate consistency with the NFW or M99 profiles, or strongly constrain or rule out the isothermal sphere model.

The most detailed form of the 'kinematical weighing' uses the distribution and kinematics of the galaxies to estimate the mass distribution, through application of the full Jeans equation of stellar dynamics (see, e.g., Binney & Tremaine 1987, BT hereafter). This method requires knowledge of the orbital characteristics of the galaxies. A first analysis along these lines was made for the Coma cluster by Kent & Gunn (1982). Merritt (1987) used the same data to estimate the orbital

anisotropy of the galaxies for various assumptions about the dependence of the mass-to-light ratio \mathcal{M}/\mathcal{L} on radius.

The shape of the mass profile of a cluster would follow directly from the projected luminosity density profile of the galaxies if the mass-to-light ratio \mathcal{M}/\mathcal{L} were constant. Evidence in favour of a constant \mathcal{M}/\mathcal{L} comes from the analyses of Carlberg, Yee, & Ellingson (1997a), van der Marel et al. (2000), and Rines et al. (2001). Carlberg et al. (2001) instead find an increasing \mathcal{M}/\mathcal{L} -profile in groups from the CNOC2 survey, while both Rines et al. (2000) and Biviano & Girardi (2003) argue for a decreasing \mathcal{M}/\mathcal{L} -profile.

The shape of the cluster \mathcal{M}/\mathcal{L} -profile seems to depend on which class of cluster galaxies is used to measure the light profile. This is hardly surprising, since the various types of galaxies are known to have different projected distributions. These differences are the result of the morphology-density relation, first described by Oemler (1974) and Melnick & Sargent (1977), and described more fully by Dressler (1980) and, lately, Thomas & Katgert (2003, paper X of this series). In clusters, this relation produces differences in the radial distribution of the various galaxy classes, and those are related to differences in the kinematics. Evidence for the relation between spatial distribution and kinematics for different cluster galaxy populations was e.g. found in the Coma cluster (Colless & Dunn 1996), in CNOC clusters at $z \approx 0.3$ by Carlberg et al. (1997b), in clusters observed in the ESO Nearby Abell Cluster Survey (ENACS, hereafter; de Theije & Katgert 1999, paper VI; Biviano et al. 2002, paper XI), as well as in other clusters (see, e.g., Mohr et al. 1996; Adami, Biviano, & Mazure 1998a). Galaxies with emission lines (ELG) provide an extreme example of the effect. The ELG are less centrally concentrated and have a higher r.m.s line-of-sight velocity than the galaxies without emission lines. This was clearly demonstrated by Biviano et al. (1997, paper III), using 75 ENACS clusters.

To study the mass profile in detail, one must combine the data for many galaxy systems, as was done by e.g., Biviano et al. (1992), Carlberg et al. (1997a, 1997b, 1997c, 2001), van der Marel et al. (2000), Biviano & Girardi (2003), and in papers III, VI, VII (Adami et al. 1998b), IX (Thomas, Hartendorp, & Katgert 2003), X, and XI of this series. For an ‘ensemble’ cluster, built from 14 clusters with redshifts between about 0.2 and 0.5, with a total of 1150 CNOC redshifts, Carlberg et al. (1997c) found that the number density profile is consistent with the NFW mass density profile. This result was confirmed with a more detailed analysis by van der Marel et al. (2000). Using the ENACS dataset, in paper VII we found that the number density profile of a composite cluster of 29 nearby ACO clusters with smooth projected galaxy distributions did not show the central cusp of the NFW mass profile, in particular when the brightest galaxies are removed from the sample. This could mean that \mathcal{M}/\mathcal{L} increases towards the center. Recently, Biviano & Girardi (2003) analysed an ‘ensemble’ cluster, built from 43 nearby clusters observed in the 2dF Galaxy Redshift Survey (Colless et al. 2001). From that sample, which has only three clusters (A957, A978 and A2734) in common with the present sample, they concluded that both cuspy profiles of the NFW and M99 form, and profiles with a core are acceptable, as long as the core radius is sufficiently small.

The above results indicate the importance of a study of the mass profile and of the radial dependence of \mathcal{M}/\mathcal{L} . In this paper we present such a study, based on a sample of rich nearby clusters observed in the ENACS. This paper is organised as follows. In § 2 we summarize the data. In § 3 we justify our choice to use the Early-type galaxies that are not in substructures as tracers of the potential. In § 4 we present the number-density and velocity-dispersion profiles of the Early-type galaxies and we describe how we obtained a non-parametric estimate of the cluster mass profile via direct solution of the Jeans equation. In § 5 we compare our result with models, and we derive the best-fit models from a comparison of the observed and predicted velocity-dispersion profiles. In § 6 we derive the radial dependence of the \mathcal{M}/\mathcal{L} -ratio, for all galaxies together and for the Early-type galaxies. In § 7 we discuss our results, which are summarized in § 8, where we also give our conclusions. In Appendix A we describe our method of interloper rejection. In Appendix B we detail the methods by which we determined the number-density, luminosity-density, and velocity-dispersion profiles. In Appendix C we review and discuss the basic assumptions made in the determination of the mass profile.

2. The data

Our determination of the mass profile of rich clusters is based on data obtained in the context of the ENACS. The multi-object fiber spectroscopy with the 3.6-m telescope at La Silla is described in Katgert et al. (1996, 1998, papers I and V of this series, respectively). In those papers, the photometry of the 5634 galaxies in 107 rich, nearby ($z \lesssim 0.1$) Abell clusters is also discussed. After the spectroscopic survey was done, CCD images were obtained with the Dutch 92-cm telescope at La Silla for 2295 ENACS galaxies. These have yielded morphological types (Thomas 2003, paper VIII), which were used to refine and recalibrate the galaxy classification based on the ENACS spectra, as carried out previously in paper VI. The CCD images also yielded structural parameters, through a decomposition of the brightness profiles into bulge and disk contributions (paper IX).

The ENACS morphological types were supplemented with morphological types from the literature, and subsequently combined with the spectral types into a single classification scheme. This has provided galaxy types for 4884 ENACS galaxies, of which 56% are morphological, 35% are spectroscopic, 6% are a combination of morphological and spectral types, and the remaining 3% were special in that they had an early morphological type (E or S0) but showed emission lines in the spectrum. These galaxy types were used to study the morphology-radius and morphology-density relations (paper X). They also form the basis of the study of morphology and luminosity segregation which uses velocities as well as positions (paper XI).

In combining the data for an ensemble of many clusters, all projected clustercentric distances were expressed in terms of r_{200} , as derived from the global velocity dispersion (see e.g. Carlberg et al. 1997c). This ensures that we avoid, as much as possible, mixing inner virialized cluster regions with external non-virialized cluster regions. Similarly, all galaxy velocities, relative to the mean velocity of their parent cluster, were expressed in terms of the global velocity dispersion of their

parent cluster, σ_p .

The ensemble cluster effectively represents each of our clusters if these form a homologous set, and if we adopted the correct scaling. An indication that clusters form a homologous set comes from the existence of a fundamental plane that relates some of the cluster global properties (Schaeffer et al. 1993; Adami et al. 1998c, paper IV of this series). As shown by Beisbart, Valdarnini, & Buchert (2001) clusters with substructure tend to deviate from the fundamental plane, thereby violating homology. The exclusion of all clusters with even a minor amount of substructure would have greatly reduced the size of the ensemble cluster. Instead, by eliminating the galaxies that in their respective clusters are in substructures, we have tried to reduce the effects of substructure in our analysis as much as possible.

In paper XI we combined the data for 59 clusters with $z < 0.1$, each with at least 20 member galaxies with ENACS redshifts, and with galaxy types for at least 80% of the members (see Table A.1 in paper XI). The ensemble cluster contains 3056 member galaxies, for 2948 (or 96%) of which a galaxy type is known. The rejection of interlopers was based on the method of den Hartog & Katgert (1996), which is summarized in Appendix A. In this ensemble cluster it was found that galaxies in substructure have different phase-space distributions from those outside substructure, and that this is true for all galaxy types.

The analysis of the mass profile cannot be based on the sample of galaxies within substructure because the members of substructure are orbiting together, so that their kinematics does not only probe the large-scale properties of the cluster potential. For the galaxies outside substructure, it was found that there are 4 galaxy classes that must be distinguished because they have different phase-space distributions. These 4 classes are: (i) the brightest ellipticals (with $M_R \leq -22 + 5 \log h$), which we refer to as 'E_{br}' in the following, (ii) the other ellipticals together with the S0 galaxies (referred to as 'Early-type' galaxies, in the following), (iii) the early spirals (Sa–Sb), which we refer to as 'S_e' in the following, and (iv) the late spirals and irregulars (Sbc–Ir) together with the ELG (except those with early morphology), globally referred to as 'S_l' in what follows.

In Table 1 we show the number of cluster members outside substructure in the 59 clusters, in each of the 4 galaxy classes defined above. As explained in Appendix B, in building the number density profiles we need to correct for sampling incompleteness. In order to keep the correction factor small, galaxies located in poorly-sampled regions are not used in the present analysis, and are not counted in Table 1.

Table 1: The numbers of galaxies outside substructure

	E _{br}	Early	S _e	S _l
	$M_R \leq -22 + 5 \log h$	$M_R > -22 + 5 \log h$		
	34	1129	177	328

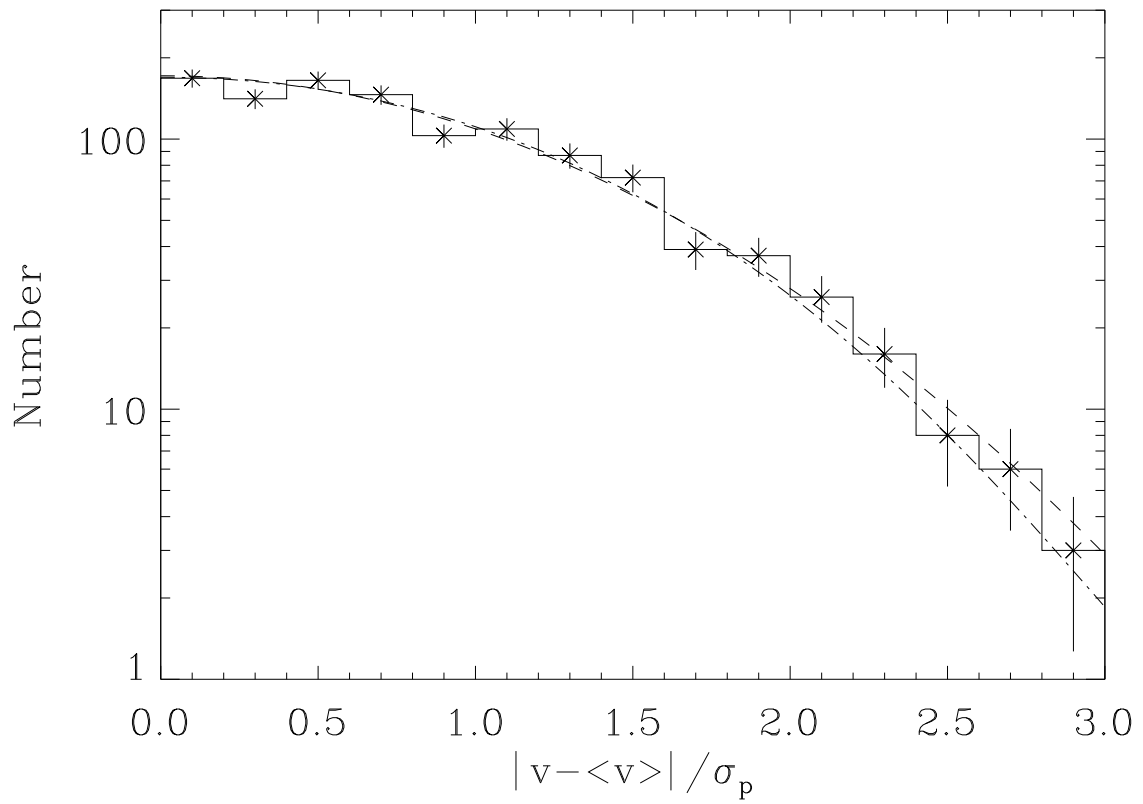


Fig. 1.— The velocity distribution of the Early-type class, with the best-fitting Gaussian (dashed-line), and the best-fitting Gauss-Hermite polynomial (dash-dotted line) superposed.

3. The Early-type galaxies as tracers of the mass profile

Since we want to derive the mass profile of the ensemble cluster by application of the Jeans equation of stellar dynamics, we must assess the suitability of each of the 4 galaxy classes to serve as tracers of the potential. To begin with, suitable tracers should be in equilibrium with the cluster potential. However, application of the Jeans equation also requires that the orbital characteristics are known or, in other words: that we have information on the (an-)isotropy of the velocity distribution.

For that reason, and in view of the results in papers III and VI, it is very unlikely that the S_1 can be used, since the analyses in these papers suggest that they may be on first-approach orbits towards the central regions. This could still mean that they are in equilibrium with the potential, but as we have no *a priori* knowledge of their orbits, except that they are unlikely to be isotropic, these galaxies do not qualify as good tracers.

The E_{DR} could, for all that we know, have an isotropic velocity distribution. However, it is unlikely that, as a class, they satisfy the basic assumption underlying the Jeans equation, namely that it describes a collisionless particle fluid. The usual interpretation that the brightest ellipticals have been directed to the central regions through dynamical friction after which they have grown at the expense of other galaxies might make them unfit for estimates of the mass profile.

As to the choice between the two remaining classes, the relative statistical weights clearly point to the use of the Early-type galaxies as tracers of the mass profile. However, in addition to this pragmatic argument there are other, more fundamental reasons for this choice. The most important one is that the stellar population in most ellipticals is quite old, and evidence is mounting that most of the ellipticals formed before they entered the cluster. This should have allowed them to settle in the potential and become good tracers of it.

As was shown in paper XI, the (R, v) -distribution of the S_0 galaxies is very similar to that of the ellipticals. At first, this may appear somewhat surprising. Although the stellar population of many S_0 galaxies is probably as old as that of the ellipticals, it is generally believed that a significant fraction of S_0 's has formed rather recently through the transformation of early spirals by impulsive encounters. Apparently, the present rate of formation of S_0 's is sufficiently low that the bulk of the transformation of early spirals has taken place sufficiently long ago, so that the phase space distribution of the S_0 's has relaxed to that of the older population of E 's.

Use of the Early-type galaxies requires that we know, or can make an educated guess about, the anisotropy of their velocity distribution. We will assume that their orbits are isotropic, and this assumption can be checked to some extent because the distribution of relative radial velocities depends on the anisotropy of the 3-D velocity distribution, as was shown by Merritt (1987) and van der Marel et al. (2000). By calculating the even-order Gauss-Hermite coefficients for the velocity distribution of the CNOC1 survey, van der Marel et al. (2000) showed that they could constrain the range of allowed values of the velocity anisotropy, from a comparison with dynamical models.

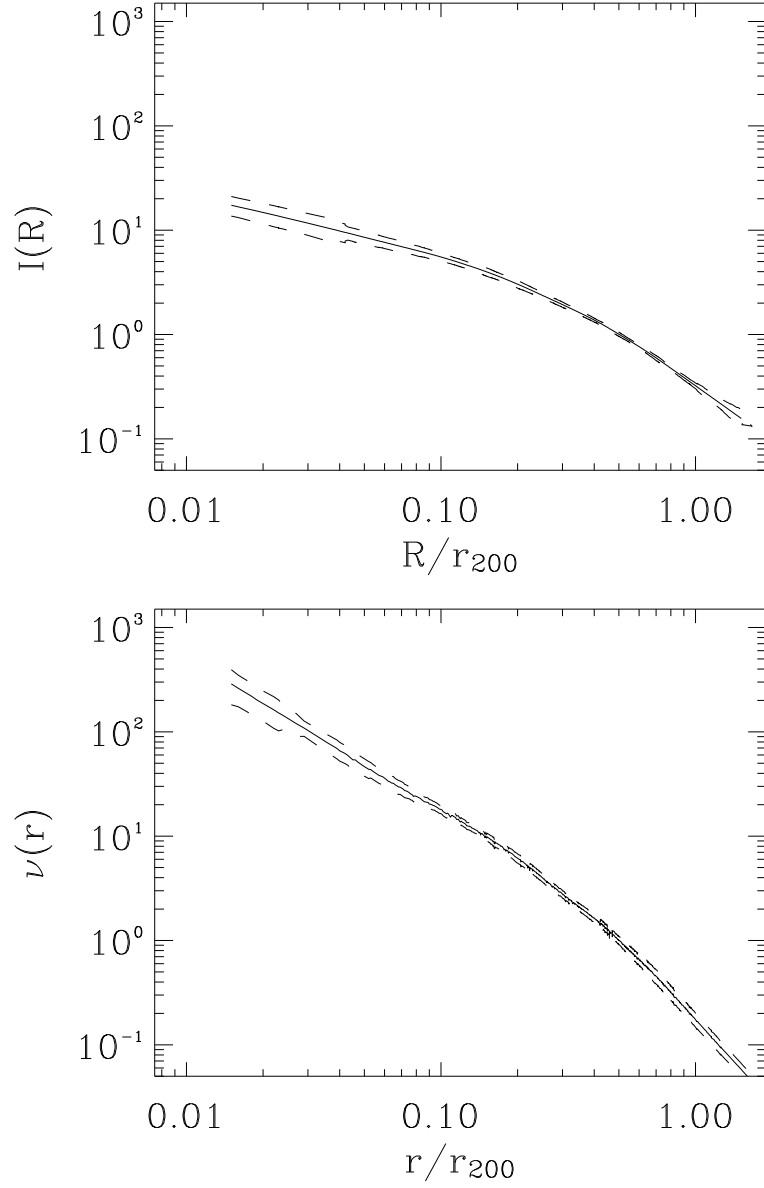


Fig. 2.— Top: The best LOWESS estimate (solid line) of $I(R)$ of the Early-type galaxies, within the $1-\sigma$ confidence interval determined from bootstrap resamplings (dashed lines). Bottom: The best estimate (solid line) of $\nu(r)$, extrapolated to $r = 6.67 r_{200}$, within the $1-\sigma$ confidence interval determined from bootstrap resamplings (dashed lines).

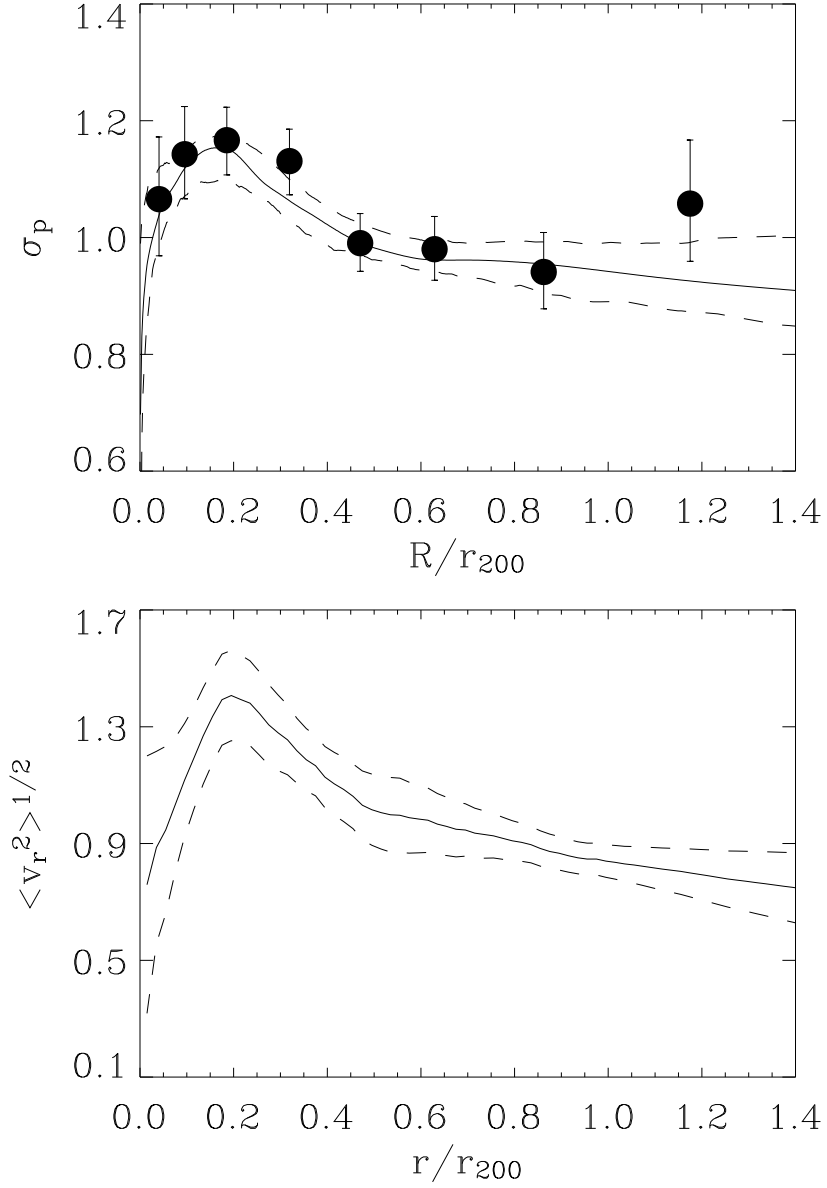


Fig. 3.— Top: The best LOWESS estimate (heavy line) of $\sigma_p(R)$ of the Early-type galaxies, with 68% confidence levels (dashed lines), together with binned estimates. Bottom: The best estimate (heavy line) of $\langle v_r^2 \rangle^{1/2}(r)$, with 68% confidence levels.

The velocity distribution of the Early-type galaxies in our ensemble cluster is shown in Fig. 1, with the best-fitting Gaussian and the best-fitting Gauss-Hermite polynomial superposed. It appears that the deviations from a Gaussian are very small. This is confirmed by the values of h_4 and h_6 , which are -0.016 and 0.005 . Although we refrain from constructing plausible distribution functions, the projected number density – and therefore also the 3-D number density – is sufficiently close to that used by van der Marel et al. (2000) that we can conclude from their Fig. 8 that our assumption $\beta(r) = 1 - \langle v_t^2 \rangle(r) / \langle v_r^2 \rangle(r) \equiv 0$ for the E+S0 class is very plausible (as a matter of fact we conclude that $-0.6 \lesssim \beta \lesssim 0.1$, or, equivalently, $0.8 \lesssim \sqrt{\langle v_r^2 \rangle / \langle v_t^2 \rangle} \lesssim 1.05$).

4. Direct solution of the Jeans equation

Application of the Jeans equation for the determination of the cluster mass profile requires two observables: the projected number-density profile $I(R)$, and the velocity-dispersion profile $\sigma_p(R)$ of the Early-type galaxies. Here we summarize the steps involved in the determination of these profiles and their inversion to the 3-D space. Details can be found in Appendix B.

For the determination of both number-density and velocity-dispersion profiles we use the LOWESS technique (Gebhardt et al. 1994). The number-density profile, $I(R)$, is corrected for sampling incompleteness. The confidence levels (c.l. hereafter) on $I(R)$ are measured via a bootstrap procedure. The projected number-density profile $I(R)$ is shown in the upper panel Fig. 2. The projected number density $I(R)$ must be deprojected to yield the 3-D number density $\nu(r)$. This deprojection is obtained via a straightforward integration of the Abel integral, which involves no assumptions, apart from the behaviour of $I(R)$ towards large radii. We checked that the deprojected profile is essentially independent from how we extrapolate $I(R)$ to large radii (see Appendix B). We show the deprojected profile $\nu(r)$ in the bottom panel of Fig. 2.

In the upper panel of Fig. 3 we show the projected velocity-dispersion profile, determined with the LOWESS technique, together with a binned version, where the value of the velocity dispersion in each radial bin is computed using the robust bi-weight estimator (see Beers, Flynn, & Gebhardt 1990).

With the estimates of $I(R)$, $\nu(r)$ and $\sigma_p(R)$ we now proceed to obtain the cluster mass profile $M(< R)$. The procedure is well-known (see, e.g., BT). We make the usual assumptions that the cluster is in steady-state, and that net rotation is negligible. With these assumptions, and in the case of spherical symmetry (see also Appendix C), the procedure is as follows. First, one must deproject $\sigma_p(R)$ to obtain $\langle v_r^2 \rangle(r)$. In other words, one should solve the integral relation:

$$I(R)\sigma_p^2(R) = 2 \int_R^\infty \left(1 - \beta(r) \frac{R^2}{r^2} \right) \frac{r\nu(r)\langle v_r^2 \rangle(r) dr}{\sqrt{r^2 - R^2}}, \quad (1)$$

where, as before:

$$\beta(r) \equiv 1 - \frac{\langle v_t^2 \rangle(r)}{\langle v_r^2 \rangle(r)}, \quad (2)$$

and $\langle v_r^2 \rangle(r)$, $\langle v_t^2 \rangle(r)$ are the mean squared components of the radial and tangential velocity. For the special case $\beta(r) \equiv 0$ the solution is:

$$\langle v_r^2 \rangle(r) = -\frac{1}{\pi\nu(r)} \int_r^\infty \frac{d[I(R) \times \sigma_p^2(R)]}{dR} \frac{dR}{\sqrt{R^2 - r^2}}. \quad (3)$$

The $\langle v_r^2 \rangle(r)$ profile and c.l. resulting from $I(R)$, $\sigma_p(R)$, and the c.l. on $\sigma_p(R)$ (see Appendix B for details) are shown in the lower panel of Fig. 3.

The mass profile then follows directly from the Jeans equation (see, e.g., BT):

$$M(< r) = -\frac{r \langle v_r^2 \rangle}{G} \left(\frac{d \ln \nu}{d \ln r} + \frac{d \ln \langle v_r^2 \rangle}{d \ln r} \right), \quad (4)$$

where β was assumed to be 0 (see § 3).

The result is shown in the upper panel of Fig. 4. Since in our ensemble cluster galaxy velocities are normalised by their cluster global velocity dispersion, σ_p , and galaxy clustercentric distances are scaled by their cluster virial radius, r_{200} , the mass is also expressed in normalised units². Also shown are the mass profiles of four popular models: viz. those of NFW, M99, the softened isothermal sphere (SIS, hereafter; see, e.g., Geller et al. 1999), and that of Burkert (1995). They are all one-parameter models in which the linear scale (in units of r_{200}) is variable. The analytic expressions are:

$$\rho_{NFW}(r) = \frac{\rho_0}{(r/r_s)(1 + r/r_s)^2} \quad (5)$$

$$\rho_{M99}(r) = \frac{\rho_0}{(r/r_M)^{1.5}[1 + (r/r_M)^{1.5}]} \quad (6)$$

$$\rho_{SIS}(r) = \frac{\rho_0}{1 + (r/r_c)^2} \quad (7)$$

$$\rho_{Burkert}(r) = \frac{\rho_0}{(1 + r/r_0)[1 + (r/r_0)^2]} \quad (8)$$

Our mass profile $M(< r)$ and the four model profiles cannot be compared directly, because the c.l. of our mass profile are only approximate (as discussed in Appendix B). For a proper statistical comparison we need to project our mass profile in the space of observables, and this is described in the next section. Yet, for the purpose of illustration, we show in the lower panel of Fig. 4 the mass density profile as derived by differentiation of the observed mass profile $M(< r)$, together with the four model density profiles. In both panels of Fig. 4 we have used the best-fit values $r_s/r_{200} = 0.25$, $r_M/r_{200} = 0.5$, $r_c/r_{200} = 0.02$, and $r_0/r_{200} = 0.15$ (see below).

As a test of our assumption about the unsuitability of the late-type galaxies as tracers of the potential (see § 3), we have also applied the procedure, described here for the Early-type galaxies,

²Since the median velocity dispersion of our cluster sample is 699 km s⁻¹, and the median value of r_{200} is 1.2 $h^{-1} Mpc$ one mass unit corresponds to $\approx 1.4 \times 10^{14} h^{-1} M_\odot$

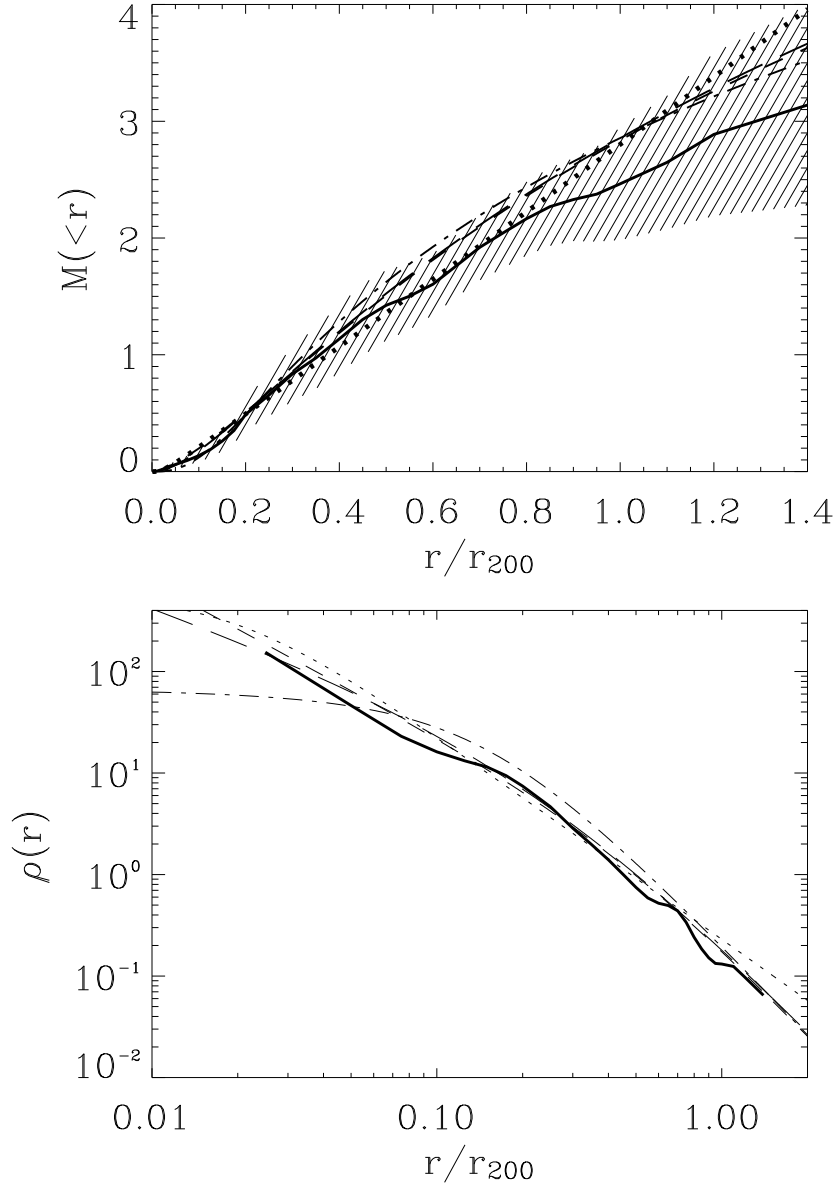


Fig. 4.— Top: The mass profile $M(< r)$ calculated from the Jeans equation, using the Early-type galaxies as tracers of the potential (heavy solid line). Isotropic orbits were assumed, and the approximate 68% confidence region is indicated by the shading. The mass scale is in arbitrary units. Also shown are the best-fit mass models of the NFW (long dashes), M99 (short dashes), SIS (dotted line) and Burkert (dash-dotted line) types. Note that the best-fit mass models were not derived from fits to $M(< r)$, but from a comparison of the observed and predicted velocity-dispersion profiles (see § 5). Bottom: the mass density profile $\rho(r)$ derived by differentiating our observed $M(< r)$ (heavy solid line) compared with the 4 models (same coding as above).

to the early and late spirals (again, assuming isotropy). The S_e mass profile is not very different from that in Fig. 4, but the S_l mass profile is considerably steeper, which supports our assumption. In a forthcoming paper (Biviano & Katgert, 2004), we discuss in detail the dynamical equilibrium (including the orbital anisotropies) of the E_{br} , S_e and S_l classes, in the potential derived here from the data of the Early-type galaxies.

5. Comparison with model mass-profiles

In order to compare our observed mass profile with models from the literature, we work in the domain of observables, viz. in $\sigma_p(R)$. This is possible because one can solve for $\langle v_r^2 \rangle(r)$ using the observed $\nu(r)$, an assumed mass profile $M(< r)$, and an assumed $\beta(r)$, as follows:

$$\nu(r)\langle v_r^2 \rangle(r) = -G \int_r^\infty \nu(\xi) \frac{M(< \xi)}{\xi^2} \exp \left[2 \int_r^\xi \frac{\beta dx}{x} \right] d\xi \quad (9)$$

This solution, given by van der Marel (1994), is a special case of a more general solution of the Jeans equation which was developed by Bacon, Simien, & Monnet (1983) for building dynamical models of elliptical galaxies. For $\beta = 0$ the above equation reduces to:

$$\nu(r)\langle v_r^2 \rangle(r) = -G \int_r^\infty \nu(x) M(< x) x^{-2} dx \quad (10)$$

Given a model mass profile, $M(< r)$, and an observed number-density profile, $\nu(r)$, it is thus possible to compute model projected velocity-dispersion profiles, through eq. 10 and the usual Abel relation.

The comparison between the model and the observed velocity-dispersion profile yields a value for χ^2 by which we measure the acceptability of the assumed mass-profile model. A straightforward determination of the χ^2 value requires the observed profile to have independent data-points. In this comparison we therefore use a binned $\sigma_p(R)$ -profile, rather than the LOWESS profile. Only the data points within the virial radius r_{200} are considered for the fit, since galaxies at larger radii might not yet have relaxed to dynamical equilibrium. The uncertainty in the observed $\nu(R)$, determined from the bootstrap resamplings of $I(R)$ (see Appendix B.1) is taken into account in the χ^2 -analysis. In practice, for each bootstrap resampling of $I(R)$ we have a corresponding $\nu(r)$, and hence, a different model velocity dispersion profile, obtained via eq. 10. This allows us to compute an r.m.s. for each point of the model velocity dispersion profile. The model r.m.s. is then added in quadrature to the uncertainty of the observed $\sigma_p(R)$ to give the full uncertainty to be used in the χ^2 -analysis.

We checked that our results are robust w.r.t. different choices of both the binning radii for $\sigma_p(R)$, and the way in which $I(R)$ is extrapolated to large radii to yield $\nu(r)$ through the Abel inversion (see Appendix B). Different choices of the $\sigma_p(R)$ binning and of the $I(R)$ extrapolation affect the best-fit values of the mass model parameters by $\lesssim 15\%$ and $\lesssim 10\%$, respectively.

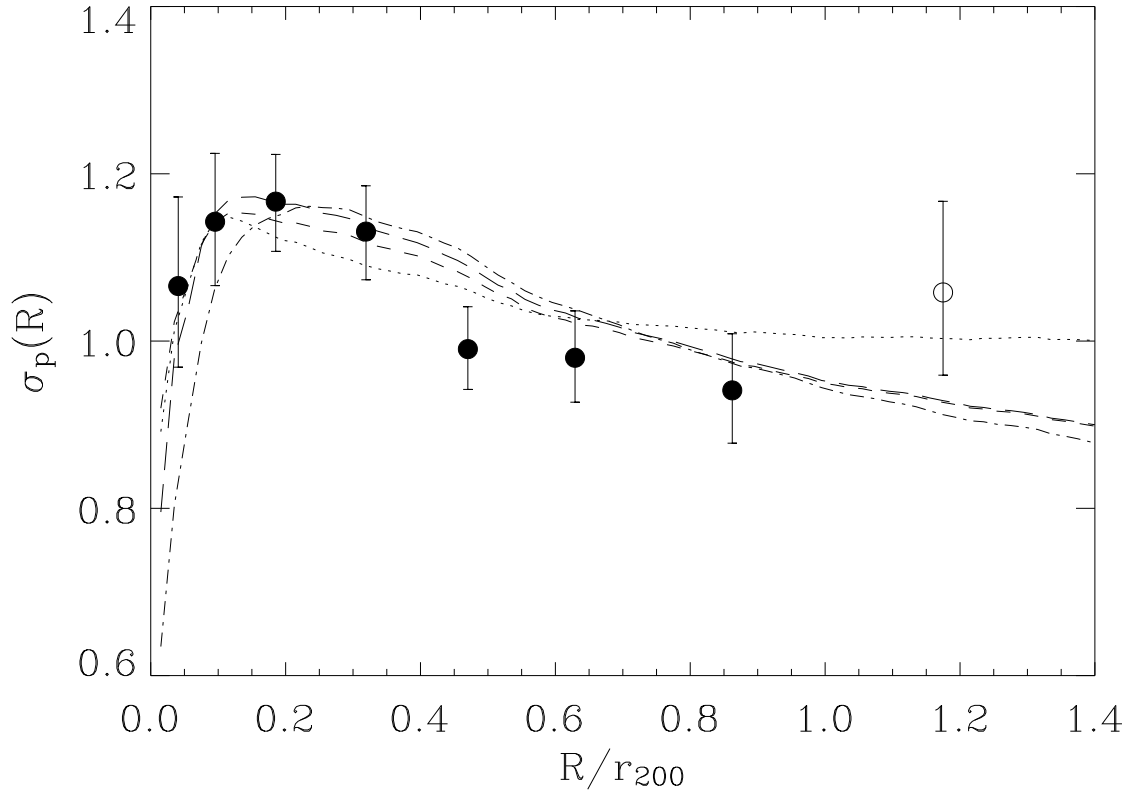


Fig. 5.— The observed velocity-dispersion profile of the Early-type galaxies (filled circles with error bars) and the four velocity-dispersion profiles predicted for the 4 mass models: NFW (long dashes), M99 (short dashes), SIS (dotted line) and Burkert (dash-dotted line). Note that the fits do not include the outermost point (open circles).

We consider two ‘cuspy’ model mass profiles (NFW and M99), and two profiles with a ‘core’ (SIS and that of Burkert 1995) – see § 3. All four model mass profiles provide acceptable fits to the observed $\sigma_p(R)$, although the models of NFW and Burkert provide marginally better fits than the M99 and, in particular, the SIS models. More specifically, using the χ^2 statistics, we estimate the rejection probabilities of the best-fit NFW, M99, SIS and Burkert models to be 19%, 28%, 72% and 11%, respectively. Note that the χ^2 values were calculated for the points with $R/r_{200} < 1.0$, because inclusion of data beyond the virial radius does not seem very sensible. As a matter of fact, if the outmost point is included all 4 models provide fits of similar quality.

The 68% c.l. range for the NFW-profile scale parameter is $0.15 \leq r_s/r_{200} \leq 0.40$, with a best-fit value of $r_s = 0.25 r_{200}$. In terms of the concentration parameter, the best-fit value is $c \equiv r_{200}/r_s = 4_{-1.5}^{+2.7}$. The 68% c.l. range for the M99-profile scale parameter is $0.30 \leq r_M/r_{200} \leq 0.75$ with a best-fit value of $r_M = 0.45 r_{200}$. On the other hand, for no value of the scale parameter r_c is the SIS model acceptable at the 68% c.l. or better. The best-fit is obtained for $r_c = 0.02 r_{200}$ and values $r_c > 0.075 r_{200}$ are rejected at $> 99\%$ c.l. The 68% c.l. range for the Burkert scale parameter r_0 is $0.10 \leq r_0/r_{200} \leq 0.18$ with a best-fit value of $r_0 = 0.15 r_{200}$. Values $r_0 > 0.25 r_{200}$ are rejected at $> 99\%$ c.l. The allowed range for the Burkert scale parameter seems larger than for the SIS scale parameter. Note, however, that the two scale parameters do not have the same meaning. If we define the core radius as the clustercentric distance where the density falls below half its central value, $r_{\rho_0/2}$, this corresponds to r_c in the SIS model, and to $\sim 0.5 r_0$ in the Burkert model. We conclude that the core models (and in particular the SIS-model) that fit our data have such small core-radii that they very much resemble the two core-less models.

In Fig. 5 we show the observed (binned) $\sigma_p(R)$ of the Early-type class, together with the velocity dispersion profiles predicted from the best-fit NFW, M99, SIS and Burkert $M(< r)$ models. For the sake of clarity, we do not show the uncertainties in the model velocity dispersion profiles related to the uncertainties in $\nu(r)$. These are however much smaller than the uncertainties of the observed velocity dispersion profile. From Fig. 5 it can be seen that the best-fit NFW and M99 models predict almost indistinguishable velocity dispersion profiles. On the other hand, fitting the inner part of $\sigma_p(R)$ requires such a small core radius for the SIS model, that the model velocity dispersion profile flattens already at $r \approx 0.4 r_{200}$, while the observed profile continues to drop. Formally, the best-fit Burkert model also provides the best fit to the observations, as it reproduces the broad maximum in $\sigma_p(R)$ better than do the other three models. However, we are somewhat suspicious of the very strong decrease of $\sigma_p(R)$ below $r \approx 0.1 r_{200}$, although it is only 2.5σ lower than the LOWESS estimate of $\sigma_p(R)$.

6. The radial variation of the mass-to-light ratio \mathcal{M}/\mathcal{L}

As mentioned in the Introduction, there is not yet a clear, unambiguous result for the dependence of \mathcal{M}/\mathcal{L} on radius in the literature, and therefore we have also used our data to derive $\mathcal{M}/\mathcal{L}(r)$. The luminosity-density profile $\mathcal{L}_{all}(r)$ was determined from the projected luminosity den-

sity profile of the galaxies with the same method used to deproject $I(R)$, except that galaxies are now weighed by their luminosities. Note that the luminosity density profile is constructed for all galaxies, both in and outside substructures. As discussed in Appendix B, $\mathcal{L}_{all}(r)$ only accounts for the luminosities of the galaxies in our sample, as we did not try to recover the luminosity of unseen cluster galaxies (e.g., by fitting a luminosity function to the observed luminosity distribution, and extrapolating beyond the completeness limit). In fact, we are not interested in estimating the absolute values of \mathcal{M}/\mathcal{L} , but only in its radial behaviour, and there is no way we could estimate $\mathcal{L}(r)$ for the total galaxy population, without actually measuring positions and luminosities of all members. The full magnitude range of the galaxies on which $\mathcal{L}_{all}(r)$ is based is $-23.3 \leq M_R - 5 \log h \leq -17.4$, with an average $\langle M_R \rangle = -20.25 + 5 \log h$, and an r.m.s. of 0.94 mag. The average absolute magnitude is about one magnitude fainter than the knee of the cluster galaxy luminosity function, M^* (e.g. Yagi et al. 2002). Note that our magnitudes are K-corrected, but that we did not apply any correction for evolutionary effects. For redshifts $\lesssim 0.1$, those are very small in R -band, and the *differential* evolutionary correction for early- and late-type galaxies is estimated to be less than 5% in luminosity.

In the upper panel of Fig. 6 we show the ratio of the total mass-density profile $\rho(r)$ of the best fitting NFW and Burkert models, and $\mathcal{L}_{all}(r)$ calculated for all galaxies, i.e. the differential mass-to-light ratio as a function of r . The shaded region shows the 68% uncertainties in the profile ratio, as calculated from the union of the 68% c.l. ranges of the best-fitting NFW and Burkert models. Note that the relative uncertainties in $\mathcal{L}_{all}(r)$ are much smaller than the allowed ranges of $\rho(r)$. The $\mathcal{M}/\mathcal{L}_{all}(r)$ -ratio is consistent with a constant value in the radial range $0.2 \leq r/r_{200} \leq 1.4$, even though there is an apparent decrease from $0.2 r_{200}$ to $0.7 r_{200}$.

However, within $0.1 r_{200}$ the $\mathcal{M}/\mathcal{L}_{all}$ -ratio is significantly lower than at larger radii. The reason for that could obviously be that the E_{br} which are much more centrally concentrated than the other galaxy classes, contribute relatively little mass for their luminosity. To check this explanation, we also determined the \mathcal{M}/\mathcal{L} -ratio for all galaxies without the E_{br} (i.e. $\mathcal{M}/\mathcal{L}_{all-brightest E}(r)$). The result is shown in the middle panel of Fig. 6. As expected, the strong decrease of the \mathcal{M}/\mathcal{L} -ratio within $0.2 r_{200}$ has largely disappeared. However, the apparent decrease of \mathcal{M}/\mathcal{L} from $0.2 r_{200}$ to $0.7 r_{200}$ is now stronger.

To enable comparison with data on high-redshift clusters, where selection of cluster members is often done using the red-galaxy sequence in the colour-magnitude diagram, we also determined the \mathcal{M}/\mathcal{L} -ratio for the Early-type galaxies only (again excluding the E_{br}); the result is shown in the lower panel of Fig. 6. The apparent decrease of \mathcal{M}/\mathcal{L} from $0.2 r_{200}$ to $0.7 r_{200}$ has disappeared, and the \mathcal{M}/\mathcal{L} -ratio for the Early-type galaxies only, is consistent with a constant value. In other words: the luminosity of the Early-type galaxies traces the total mass very well. Therefore, we conclude that to first order, the $\mathcal{M}/\mathcal{L}(r)$ -profile can be understood as a flat profile due to the Early-type galaxies, which is modified by the 'extra' luminosity of the E_{br} within $0.2 r_{200}$, and by the luminosity of the spirals beyond $0.2 r_{200}$.

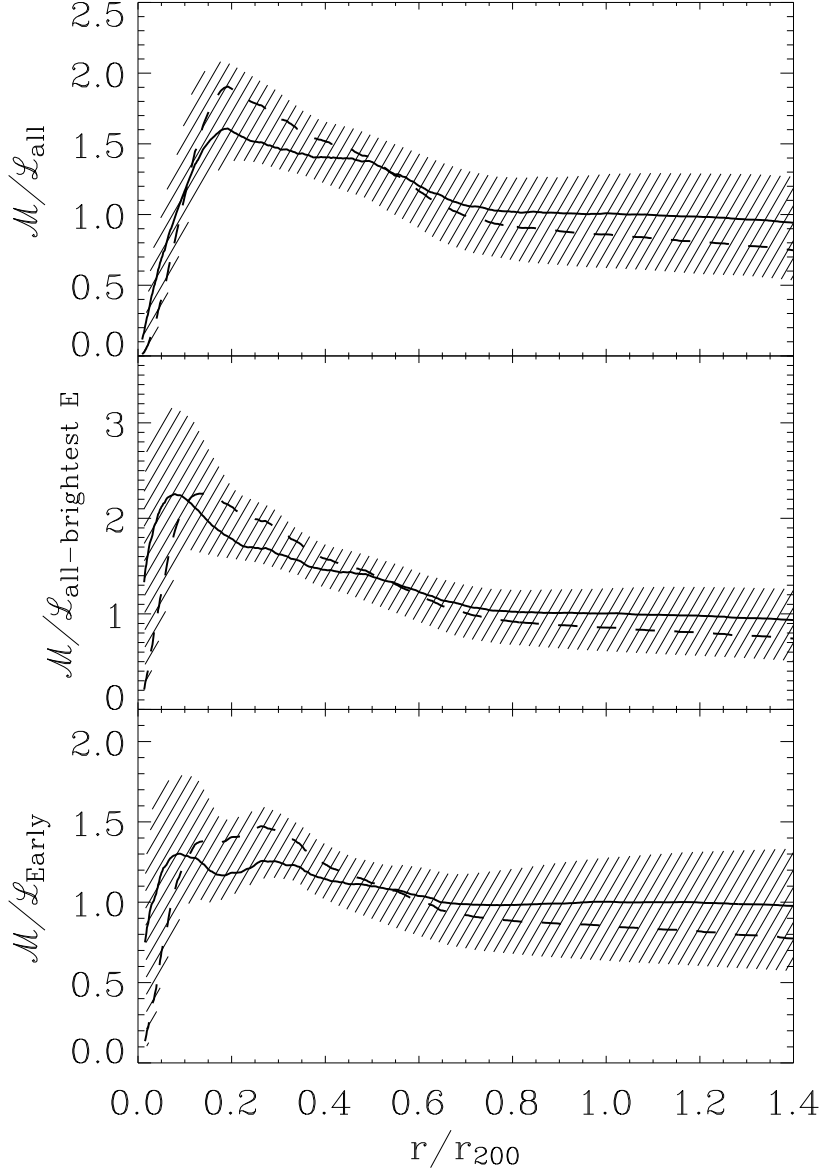


Fig. 6.— Top: $\mathcal{M}/\mathcal{L}(r)$ -profile, normalized at r_{200} , and calculated as $\rho(r)/\mathcal{L}_{all}(r)$ for all galaxies in our sample. $\mathcal{L}_{all}(r)$ is the deprojected 3-D luminosity profile and $\rho(r)$ corresponds to the best-fitting NFW (solid line) and Burkert (dashed line) models. The shaded region denotes the 68% uncertainties in the profile ratio, as calculated from the union of the 68% c.l. ranges of those models. Center: $\mathcal{M}/\mathcal{L}(r)$ -profile for all galaxies except the brightest ellipticals, expressed in normalized units and calculated as $\rho(r)/\mathcal{L}_{all-brightest E}(r)$. The 68% uncertainties in the profile ratio are calculated as described above. Bottom: $\mathcal{M}/\mathcal{L}(r)$ -profile, expressed in normalized units and calculated as $\rho(r)/\mathcal{L}_{Early}(r)$ for the Early-type galaxies only. The 68% uncertainties in the profile ratio are calculated as described above.

7. Discussion

7.1. The Mass Profile

Using the ENACS data-set complemented with recently obtained morphological data, we determined the mass and mass-to-light profile for an ‘ensemble’ cluster built from 59 nearby clusters. Following the results of the analysis of paper XI, the sample of cluster galaxies was divided into four classes, viz. the brightest ellipticals (E_{br}), the Early-type galaxies (the other ellipticals and the S0 galaxies), and the early and late spirals. We used the Early-type class to obtain a non-parametric estimate of the mass profile through the application of the Jeans equation (see § 4), and we fitted mass-profile models (see § 5). In these analyses, we assumed isotropic orbits for the Early-type galaxies, which is supported by a Gauss-Hermite polynomial decomposition of their velocity distribution.

Both ‘cuspy’ models, like the NFW and M99 mass models, and models with a core, like the SIS and that proposed by Burkert (1995), provide acceptable fits to the data. This follows from a comparison of the observed and predicted velocity-dispersion profile of the Early-type galaxies. However, the best-fit core models have such small core-radii that they are not too different from the cuspy models. In other words, we did not find compelling evidence for the existence of a ‘core’ in the matter distribution in clusters.

This result, which applies to our ‘ensemble’ cluster is consistent with several previous results based on smaller cluster samples, and obtained by various methods. Among the latter are those based on an analysis of the distribution and temperature of the X-ray emitting gas (e.g. Markevitch et al. 1999; Allen et al. 2002; Arabadjis, Bautz, & Garmire 2002; Pratt & Arnaud 2002), those based on an analysis of the weak-lensing distortion of background galaxies (e.g. Lombardi et al. 2000; Clowe et al. 2000; Clowe & Schneider 2001; Athreya et al. 2002; Hoekstra et al. 2002; King et al. 2002; Dahle, Hannestad, & Sommer-Larsen 2003), and those based on an analysis of the projected phase-space distribution of the galaxies (e.g. Geller et al. 1999; van der Marel et al. 2000; Rines et al. 2002; Biviano & Girardi 2003). In some of these analyses, not only was consistency with an NFW-type mass profile established, but an upper limit to the size of a core could also be given (e.g., Arieli & Rephaeli 2003; Dahle et al. 2003). Yet, some clusters also show a sizeable core (Shapiro & Iliev 2000; Etti et al. 2002; Sand et al. 2002).

Since most of these studies are based on small numbers of clusters, it is possible (if not likely) that individual clusters have different types of mass profile. If so, the result of our analysis is that *on average* rich clusters are characterized by cuspy profiles, and that, if clusters with cores do exist, they must be a minority. It is noteworthy that the two previous analyses involving ‘ensemble’ clusters, drawn from the CNOC and the 2dFGRS datasets respectively (by van der Marel et al. 2000, and by Biviano & Girardi 2003), give a similar result. As a matter of fact, the best-fit value of the NFW scale parameter obtained in these studies ($r_s/r_{200} = 0.24$ and $r_s/r_{200} = 0.18$), is fully consistent with our value of $r_s/r_{200} = 0.25^{+0.15}_{-0.10}$.

Our result, that *on average* rich clusters have cuspy mass profiles in the central region, is in agreement with predictions of hierarchical Cold Dark Matter (CDM, hereafter) models. Our data do not allow us to choose between different predictions, like the NFW and M99 models. Apart from the fact that the latter differ only slightly, the differences are limited to the central region, where the (baryonic) mass contribution of the cD is dominant (when present). Proper comparison would require the analysis of the internal velocity dispersion of the cD (Kelson et al. 2002). In any case, recent results from numerical simulations suggest that the concept of a universal inner slope of the mass profile might be inappropriate, as dark halo mass profiles do not seem to converge to a single central power-law shape (Power et al. 2003).

The allowed range $r_s/r_{200} = 0.25^{+0.15}_{-0.10}$, that we obtain for our ensemble cluster brackets the value predicted for a rich cluster halo in a Λ CDM cosmology, $r_s/r_{200} \simeq 0.16$ (see Fig.6 in NFW). Note however, that we determine the profile of *total* cluster mass, and not only of the *dark* mass. Our result therefore includes the contribution of baryons, i.e. of galaxies and the ICM. The latter can be a substantial fraction of the total mass (e.g. Ettori, Tozzi, & Rosati 2003). Since the ICM is less centrally concentrated than the dark mass (see, e.g., Markevitch & Vikhlinin 1997; Pratt & Arnaud 2002), one expects the total mass distribution to be less concentrated than the dark mass. That might be the reason why our best-fit NFW r_s value is slightly larger than the theoretical prediction (although not significantly so). On the other hand, the baryonic mass contribution of the cD in the cluster center has the opposite effect, namely of making the total mass distribution *more* centrally concentrated than that of the dark mass (Kelson et al. 2002; Dahle et al. 2003). However, separation of the different components of the mass profile (although important) is beyond the scope of this paper.

Cosmological simulations predict an increase of r_s with the mass of the system (NFW), and therefore a decrease of r_s with redshift of the system (Bullock et al. 2001). The predicted changes are rather small; r_s/r_{200} increases by only $\sim 25\%$ over a decade in cluster mass, while from $z = 0$ to $z \approx 0.5$ it decreases by a similar amount. Comparing our low- z , 68% c.l. range of r_s/r_{200} with the value obtained for the CNOC clusters studied by van der Marel et al. (2000), of similar mass but at higher redshifts ($0.17 \leq z \leq 0.55$), we find no redshift dependence of r_s/r_{200} . Comparing our 68% c.l. r_s/r_{200} -range with the value of $\simeq 0.18$ for the poor clusters studied by Biviano & Girardi (2003), with masses 3 times smaller than ours, and with the value of $\simeq 0.13$ for the groups studied by Mahdavi et al. (1999), with masses 13 times smaller than ours, we find a trend that is qualitatively in agreement with the theoretical prediction, but which is not statistically significant.

The upper limit that we obtain for the size of a possible core provides a constraint for the cross-section of Self-Interacting Dark Matter (SIDM) models. SIDM models have become popular in recent years as a means to explain the rotation curves of low surface brightness galaxies (see, e.g., Firmani et al. 2000). We translate the constraints on the scale parameters of the SIS and Burkert models, by using the results of the simulations of Meneghetti et al. (2001, see their Table 1), and their definition of the core radius. Our results imply an upper limit to the scattering cross-section of dark matter particles of $\sigma_\star < 1 \text{ cm}^2 \text{ g}^{-1}$ at $> 99\%$ c.l., in good agreement with the conclusions

of Meneghetti et al. (2001).

7.2. The Mass-to-Luminosity Density Profile $\mathcal{M}/\mathcal{L}(\mathbf{r})$

Using the magnitudes of the ENACS galaxies, together with the best-fitting ‘cusp-’ and ‘core-’ mass models, we have studied the radial variation of the \mathcal{M}/\mathcal{L} -ratio. When the luminosity is based on all galaxies together, the \mathcal{M}/\mathcal{L} -ratio increases strongly from $r = 0$ to $0.2 r_{200}$, decreases somewhat from $0.2 r_{200}$ to $0.7 r_{200}$ and is constant beyond $0.7 r_{200}$. The strong decrease to very low values of \mathcal{M}/\mathcal{L} within $0.2 r_{200}$ is found to be largely due to the E_{br} , i.e. the brightest ellipticals with $M_R \leq -22 + 5 \log h$, because it disappears when the latter are excluded. Similarly, the decrease of \mathcal{M}/\mathcal{L} from $0.2 r_{200}$ to $0.7 r_{200}$ largely disappears when the early and late spirals are excluded. Thus, the total mass density is traced remarkably well by the Early-type (elliptical and S0) galaxies. Although the Early-type galaxies are the dominant population in present-day clusters, it does not follow automatically that their luminosity should trace the total mass so well.

As a matter of fact, the *virial* mass profile, estimated assuming that the mass density is proportional to the number density of the Early-type galaxies (see e.g. Girardi et al. 1998), generally overestimates the mass, when compared with our solution in Fig. 4 (by as much as a factor of 2, although it is reduced, but does not disappear, when a correction is made for the pressure term, see The & White 1986). A similar virial-mass bias was found by Carlberg et al. (1997b) for the CNOC clusters.

Several previous studies also yielded a flat or nearly-flat cluster \mathcal{M}/\mathcal{L} -profile when only early-type or red galaxies were selected (e.g. Carlberg et al. 1997a; van der Marel et al. 2000; Rines et al. 2001; Hoekstra et al. 2002; Biviano & Girardi 2003; Ettori & Lombardi 2003). However, near the cluster center, where the inclusion of the very bright galaxies in the sample lowers the cluster \mathcal{M}/\mathcal{L} -value, the deviation from the flat profile was noted before (see, e.g., Athreya et al. 2002). Outwardly decreasing \mathcal{M}/\mathcal{L} -profiles are generally obtained if only late-type or blue galaxies are considered (Carlberg et al. 1997b; Biviano & Girardi 2003). However, using the red photometric band, Rines et al. (2000) found a steeply decreasing \mathcal{M}/\mathcal{L} -profile in A576. Currently, the \mathcal{M}/\mathcal{L} -profiles of groups is still controversial, because it is difficult to derive a mass profile for those systems (e.g. Mahdavi et al. 1999; Carlberg et al. 2001).

Two competing processes affect the relative distributions of mass and luminosity in a cluster: viz. dynamical friction, and tidal stripping. According to Mamon (2000) and Takahashi et al. (2002) the effect of tidal stripping should dominate over the effect of dynamical friction, so that massive galaxies sink toward the cluster center but lose their halos due to tidal stripping. The result is an \mathcal{M}/\mathcal{L} -value that increases towards the cluster center. This effect is also observed in numerical simulations (Ghigna et al. 1998). Luminosity segregation of the very massive galaxies can result at an early epoch of the cluster formation (Governato et al. 2001). The fact that we do not find significant segregation of the cluster ellipticals and S0s with respect to the cluster mass (if

we exclude the very bright ellipticals) suggests that tidal stripping is able to remove the dark haloes of these galaxies, but not to affect the galaxies luminosities very much. If tidal stripping affected the luminosities, of the Early-type galaxies, we should expect a decrease of their mean luminosity towards the center, but our data do not show such a trend (see paper XI). This is also consistent with the finding of Natarajan, Kneib, & Smail (2002b), based on a gravitational lensing analysis of six galaxy clusters, that the typical halo truncation radius of cluster galaxies is 5–10 times larger than the optical radius.

8. Summary and conclusions

We have determined the mass profile of an 'ensemble' cluster built from 59 nearby clusters from the ESO Nearby Abell Cluster Survey. In this ensemble cluster, we distinguished four different classes of galaxies, viz. the brightest ellipticals (E_{br} , with $M_R \leq -22 + 5 \log h$), the Early-type galaxies, and early and late spirals, because they have significantly different projected phase-space distributions. Galaxies in substructures were excluded from the analysis.

Because the Early-type galaxies have a nearly isotropic velocity distribution we derived a non-parametric estimate of the cluster mass profile from their number-density and velocity-dispersion profiles, through the Jeans equation of stellar dynamics. We compared our result with models for the mass profile of dark matter halos, viz. the NFW, M99, SIS and Burkert models. From a comparison of observed and predicted velocity-dispersion profiles of the Early-type galaxies, it appears that all 4 mass models provide acceptable fits to the data. The best-fitt NFW model has a concentration parameter of $c = 4_{-1.5}^{+2.7}$ (68% confidence level), in agreement with results from numerical simulations. The (SIS and Burkert) core-models are only acceptable if their core-radius is sufficiently small (i.e. $r_{\rho_0/2} \lesssim 0.13 r_{200}$ at the 99% c.l.).

The \mathcal{M}/\mathcal{L} -ratio of the Early-type galaxies is remarkably independent of radial distance. The \mathcal{M}/\mathcal{L} -ratio of all galaxies together is not constant, and within $0.2 r_{200}$ it shows a strong decrease towards the cluster center, which is due to the E_{br} . The spirals cause a mild decrease of the \mathcal{M}/\mathcal{L} -ratio towards larger radii.

Our results support CDM models for the build-up of galaxy clusters, and put an upper limit to the cross-section of any SIDM that could dominate the cluster gravitational potential. We caution that our results only apply to the total mass profile, since in our analysis we cannot disentangle the baryonic and dark matter components. Subtracting the ICM component would make the mass profile steeper, but subtracting the contribution of the central cD (which is present in many of the 59 clusters) would make it shallower.

We thank Tom Thomas, Gary Mamon, and Srdjan Samurović for useful discussions. AB acknowledges the hospitality of the Leiden and Marseille Observatories. PK acknowledges the hospitality of the Trieste Observatory. This research was partially supported by the Leids Kerkhoven-

Bosscha Fonds, Leiden Observatory, and the Italian Ministry of Education, University, and Research (through MIUR grant COFIN2001028932 "Clusters and groups of galaxies, the interplay of dark and baryonic matter").

A. The rejection of interlopers

It is obviously very important that the analysis of the mass profile is done on galaxy samples from which the non-members have been removed. We identify non-members (or interlopers) with the procedure devised by den Hartog & Katgert (1996). This procedure is based on an iterative determination of an 'interim' mass profile, with which galaxies that have relative line-of-sight velocities that are inconsistent with their projected position and with the mass profile can be found. The procedure is quite conservative in that it does not eliminate cluster members, while galaxies outside the turn-around radius can be recognized quite easily. The performance of the method was checked on numerical models of galaxy clusters by van Kampen (1994; see also van Kampen 1995) which describe a two-component ensemble of galaxies and dark matter.

The procedure requires a minimum number of galaxies to start with, because the interim mass profile needs to be sufficiently well defined that the elimination of interlopers is meaningful. In practice, den Hartog & Katgert found that if the number of galaxies is less than about 45, the iterative procedure quite often does not converge, while for 45 galaxies or more the convergence generally is quite fast. We applied the method to the clusters in our sample which have at least 45 galaxies with redshifts. For the clusters with less than 45 galaxies with redshifts, we used the interloper identification of the 'richer' clusters in a statistical sense.

Since the interloper rejection method is blind to galaxy morphologies, the statistical definition of the separation between members and interlopers does not require us to limit ourselves to clusters with sufficient morphological data. Therefore we used 79 clusters with more than 45 galaxies with redshifts, of which 32 are from ENACS and 47 from the literature. In the upper panel of Fig. 7 we show the 671 interlopers identified with the method of den Hartog & Katgert (1996) in these 79 clusters, which contain a total of 8829 galaxies. At each projected radial distance R there is a well-defined lower limit to the velocity distribution of the interlopers. In the lower panel of the same figure we show the 8158 galaxies that were accepted as member galaxies. In both panels, we draw the same caustic that we visually defined as a good separation between the two subsets. Note that the inclusion of data from the literature helps defining the caustic, as the ENACS data are mostly restricted to the inner $\sim 1.5 r_{200}$.

The caustic defined in this way was used for the identification of the interlopers in clusters with less than 45 galaxies. Because we transfer the caustic in the $(R/r_{200}, |v - \langle v \rangle| / \sigma_p)$ -plane, the criterion for removing interlopers is not systematically different for the two sets of clusters.

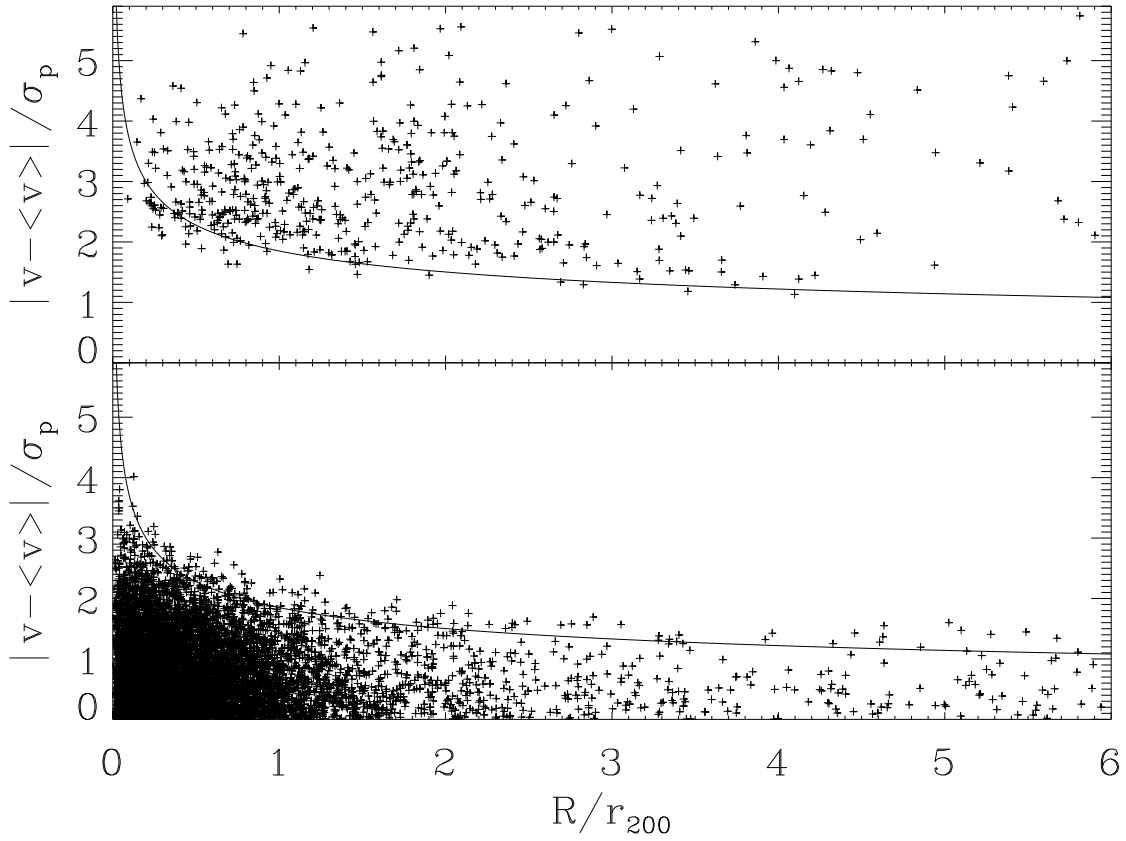


Fig. 7.— The distribution w.r.t. R/r_{200} and $|v - \langle v \rangle| / \sigma_p$ of the galaxies identified as interlopers (top) and members (bottom) in 79 clusters with at least 45 galaxies with redshift.

B. The density and velocity dispersion profiles

B.1. Number- and luminosity-density profiles

We determine the projected number density profiles $I(R)$ for the galaxy classes discussed in § 2 as follows. Because the Jeans equation requires the logarithmic derivative of the deprojected number density profile, $\nu(r)$, a smooth representation of $\nu(r)$ is needed. This is most easily obtained if the estimate of $I(R)$ is also smooth, i.e. not binned. In order to obtain a smooth estimate of $I(R)$ we have developed a variant of the LOWESS technique, which was originally designed by Gebhardt et al. (1994) to produce smooth velocity dispersion profiles.

The galaxies are ordered in increasing projected distance R . At the position of each galaxy the density $I(R)$ is calculated as the inverse of the distance between the n -th neighbours on either side. A density estimate typically involves about 10 galaxies. A smoothed version of these densities is produced with the LOWESS routine, through a weighted linear fit at each galaxy position, which uses between 30 and 80% of all densities, but with a weight that steeply drops at large distances from the galaxy in question. We chose the LOWESS smoothing factor guided by the binned versions of $I(R)$.

In the estimation of $I(R)$, each galaxy has a weight associated. This is because the ENACS spectroscopy was done with circular plug-plates used to position the fibers. Even if a cluster was observed with a single plate, this was not necessarily centered on what, after the spectroscopy, turned out to be the cluster center. The resulting azimuthal incompleteness, which at large projected distances can actually be quite severe (see e.g. Fig. 10 in paper I), depends only on the positioning of the plate(s) with respect to the cluster center, and can be easily calculated. Assuming azimuthal symmetry, which should be a good approximation for the ensemble cluster, we derived this so-called Optopus weight, which is the inverse of the fraction of the azimuth covered in the parent cluster of the galaxy, at its projected distance. Galaxies beyond the distance where the Optopus weight gets larger than 3.33 are ignored in the analysis of the mass profile.

The Optopus weight was multiplied by a second weight, which takes into account the fact that in the ensemble cluster, not all clusters do contribute at large projected distances R/r_{200} . If not properly accounted for, this incompleteness effect would produce an artificial steepening at larger radii. The correction for this effect assumes that in the radial range where a cluster does not have data, its contribution can be ‘invented’ from the clusters that *do* have data, as first described by Merrifield & Kent (1989). In our application of the method we invent data only from measured data, and not from data that are themselves (partly) invented.

We check the consistency of the smoothed $I(R)$ with 64 bootstrap resamplings of the data, because the latter give a good idea of the range of $I(R)$ ’s implied by our data. The results are shown in Fig. 2 (upper panel). We show the best LOWESS estimate (heavy line), within the 68% confidence interval determined from the 64 bootstrap resamplings (dashed lines).

We determine the deprojected profile, $\nu(r)$, for each of the 64 bootstrap resamplings of $I(R)$, through the standard Abel deprojection equation (see, e.g., BT), viz.

$$\nu(r) = -\frac{1}{\pi} \int_r^\infty \frac{dI}{dR} \frac{dR}{\sqrt{R^2 - r^2}} \quad (\text{B1})$$

via numerical integration. The deprojection requires knowledge of the $I(R)$ to arbitrarily large R . In practice, we set the upper limit of the integral equal to $R_t \equiv 6.67 r_{200}$ (it corresponds to $\sim 10h^{-1}$ Mpc for a massive cluster), since this is sufficiently far from the last measured point. We use the following smooth parametric function for the extrapolation of $I(R)$,

$$I(R \geq R_t) = C \frac{(R_t - R)^a}{R^b}. \quad (\text{B2})$$

where R_t is the largest value of R among the galaxies in the sample. Continuity of $I(R)$ and its derivative at the last measured point, R_t , fixes the values of the parameters C and b , while the shape of the extrapolation depends on the value of a . However, it turns out that for $0.5 < a < 2.0$ the detailed form of the extrapolation is not important, as different values of a lead to changes in $\nu(r)$ which, when projected, produce variations in $I(R)$ which are much smaller than the intrinsic uncertainties (as indicated by the bootstrap resamplings).

The deprojected number density profile so obtained is shown in Fig. 2 (lower panel) for $a = 1$. We show the best estimate (heavy line) within the $1\text{-}\sigma$ confidence interval determined from the 64 bootstrap resamplings (dashed lines).

The same procedure is adopted for the determination of the luminosity-density profiles, $\mathcal{L}(r)$, but with an additional weight proportional to the luminosity of each galaxy, $10^{-0.4M_R}$, where M_R is the absolute magnitude. In Paper V we have shown that the ENACS galaxy samples form unbiased subsets of the (magnitude-complete) COSMOS catalogue (e.g. Wallin et al. 1994) as far as position is concerned, so that there is no magnitude-dependent bias in the selection of the galaxies in the ENACS spectroscopic sample. It is important to note, however, that we do not estimate the *total* cluster luminosity-density, since this would require the determination of the cluster luminosity function and its extrapolation beyond the observed magnitude range.

In the Jeans equation (eq. 4) knowledge of the logarithmic derivative $d \ln \nu / d \ln r$ is needed. We determine it by fitting straight lines to the $\ln \nu$ vs. $\ln r$ data-points within intervals of $0.1 r_{200}$ width, spaced by $0.1 r_{200}$. The procedure is repeated for each of the 64 bootstrap estimates of $\nu(r)$, thus allowing us to estimate the r.m.s. of the values of the fitted line slopes, and hence the confidence levels on $d \ln \nu / d \ln r$. We checked for consistency that this estimate of $d \ln \nu / d \ln r$ is close to the direct (smoothed) numerical differentiation of $\ln \nu(r)$.

B.2. Velocity dispersion profiles

In order to determine the function $\langle v_r^2 \rangle(r)$ for a galaxy class with zero velocity-anisotropy, we need to deproject the observed line-of-sight velocity dispersion profile $\sigma_p(R)$, via the Abel equation

(see, e.g., BT),

$$\langle v_r^2 \rangle(r) = -\frac{1}{\pi\nu(r)} \int_r^\infty \frac{d[I(R)\sigma_p^2(R)]}{dR} \frac{dR}{\sqrt{R^2 - r^2}}, \quad (\text{B3})$$

which requires a smooth estimate of the product $I(R)\sigma_p^2(R)$. We determine $\sigma_p(R)$ using the LOWESS technique, with a smoothing length chosen to ensure consistency with the binned estimate of $\sigma_p(R)$. Here, galaxies beyond r_{200} are not used, since some of them could be out of equilibrium, which could bias the estimate of the cluster velocity dispersion. The σ_p -profile is shown in Fig. 3. We show the best LOWESS estimate (heavy line), within the 68% confidence interval (dashed lines; determined with 1000 Montecarlo simulations in the LOWESS program, see Gebhardt et al. 1994), as well as the binned estimates.

After extrapolating the observed $\sigma_p(R)$ to R_t , we deproject $I(R)\sigma_p^2(R)$ to obtain $\langle v_r^2 \rangle(r)$ through eq. B3. The inversion is also done for 64 of the Montecarlo simulations of $\sigma_p(R)$, in order to obtain the confidence intervals in $\langle v_r^2 \rangle(r)$ (shown in Fig. 3). We did not include the uncertainties in $I(R)$, since the uncertainties in $I(R)\sigma_p^2(R)$ are dominated by the uncertainties in $\sigma_p^2(R)$.

In the determination of $d \ln \langle v_r^2 \rangle / d \ln r$ and its confidence levels, we followed the same procedure that we used for $d \ln \nu / d \ln r$ (see Appendix B.1). The confidence levels are obtained by running the same procedure on the 64 $\langle v_r^2 \rangle$ profiles obtained from the Montecarlo simulations. We check for consistency that the $d \ln \langle v_r^2 \rangle / d \ln r$ obtained by this procedure is close to the smoothed estimate of the numerical differentiation of $\langle v_r^2 \rangle(r)$.

From the $d \ln \nu / d \ln r$, $\langle v_r^2 \rangle$, and $d \ln \langle v_r^2 \rangle / d \ln r$ profiles, we finally determine the mass profile via the Jeans equation (eq. 4). The c.l. on the mass profile immediately follow from the c.l. of the individual terms of the equation, under the simplified assumption of mutually independent errors. Such an assumption is certainly too simplistic, but all we want to achieve is a rough estimate of the mass profile c.l., to be used for illustration purposes only.

C. The ensemble cluster, and its implied properties

When combining several clusters together, it is important that the centers of all individual clusters are determined with sufficient accuracy and in a uniform manner. We followed the procedure described in paper III of this series, i.e. we used in decreasing order of preference the X-ray center, the position of the brightest cluster member near the center, the peak in the galaxy distribution, or the biweight average of the positions of all galaxies. The positions of the adopted centers are given in Table A.1 in paper XI.

In our analysis, we assume that the ensemble cluster is not rotating. Such an assumption is probably valid for individual clusters. Rotational motions are expected (and observed) in the collisional component of clusters (the intra-cluster gas) as a consequence of cluster mergers (Dupke & Bregman 2001), but not in the collisionless components (galaxies and dark matter; see Roettiger

& Flores 2000). Velocity gradients have been reported in clusters but they have not been interpreted as a signature for rotation (e.g. Biviano et al. 1996; den Hartog & Katgert 1996).

Another assumption we make is that of steady state. This is likely to be a valid assumption for *nearby* clusters. In fact, according to Ellingson et al. (2001) the infall rate of field galaxies in clusters at recent epochs is negligible (probably less than 1% in the last 2 Gyr). Moreover, Girardi & Mezzetti (2001) found no indication of evolution in the density and velocity dispersion profiles of galaxy clusters between $z \sim 0$ and $z \sim 0.3$. Finally, in the currently favoured low- Ω_m cosmology, merging and matter accretion from surrounding filaments is expected to have stopped long ago, leaving the time for clusters to dynamically relax (e.g. Plionis 2002).

We also assume spherical symmetry. While individual clusters depart from spherical symmetry, the 'ensemble' cluster is spherically symmetric by construction. An analysis of cluster ellipticities is beyond the scope of this paper, but we expect them not to be very large for the following reasons. First, our clusters are rich, and de Theije, Katgert, & van Kampen (1995) showed ellipticity to decrease significantly with increasing richness, reaching a value of ~ 0.2 for Abell richness $\gtrsim 80$. Second, our clusters are nearby, and both Melott et al. (2001) and Plionis (2002) showed cluster ellipticity to decrease with decreasing redshift, reaching ~ 0.3 at $z \sim 0.05$. Third, we only considered the inner, virialized parts of clusters, where the tidal elongation and the effects of accretion from the surrounding Large Scale Structure are less conspicuous (e.g. Melott et al. 2001; West & Bothun 1990).

REFERENCES

- Adami, C., Biviano, A., & Mazure, A. 1998a, A&A, 331, 439
- Adami, C., Mazure, A., Biviano, A., Katgert, P., Rhee, G. 1998c, A&A, 331, 493 (paper IV)
- Adami, C., Mazure, A., Katgert, P., Biviano, A. 1998b, A&A, 336, 63 (paper VII)
- Allen, S. W., Ettori, S., & Fabian, A. C. 2001, MNRAS, 324, 877
- Allen, S. W., Schmidt, R. W., & Fabian, A. C. 2002, MNRAS, 335, 256
- Arabadjij, J. S., Bautz, M. W., & Garmire, G. P. 2002, ApJ, 572, 66
- Arieli, Y., & Rephaeli, Y. 2003, New A, 8, 517
- Athreya, R. M., Mellier, Y., van Waerbeke, L., Pelló, R., Fort, B., & Dantel-Fort, M. 2002, A&A, 384, 743
- Bacon, R., Simien, F., & Monnet, G. 1983, A&A, 128, 405
- Beers, T. C., Flynn, K., & Gebhardt, K. 1990, AJ, 100, 32

- Beisbart, C., Valdarnini, R. & Buchert, T. 2001, *A&A*, 379, 412
- Binney, J. & Tremaine, S. 1987, *Galactic Dynamics* (Princeton: Princeton University Press) (BT)
- Biviano, A., Durret, F., Gerbal, D., Le Fèvre, O., Lobo, C., Mazure, A., & Slezak, E. 1996, *A&A*, 311, 95
- Biviano, A. & Girardi, M. 2003, *ApJ*, 585, 205
- Biviano, A., Girardi, M., Giuricin, G., Mardirossian, F., & Mezzetti, M. 1992, *ApJ*, 396, 35
- Biviano, A., Katgert, P. 2004, *A&A* (to be submitted)
- Biviano, A., Katgert, P., Mazure, A., Moles, M., den Hartog, R., Perea, J., & Focardi, P. 1997, *A&A*, 321, 84 (paper III)
- Biviano, A., Katgert, P., Thomas, T., & Adami, C. 2002, *A&A*, 387, 8 (paper XI)
- Bullock, J. S., Kolatt, T. S., Sigad, Y., Somerville, R. S., Kravtsov, A. V., Klypin, A. A., Primack, J. R., Dekel, A. 2001, *MNRAS*, 321, 559
- Burkert, A. 1995, *ApJ*, 447, L25
- Campusano L. E., Kneib, J-P. & Hardy, E., 1998, *ApJ*, 496, L79
- Carlberg, R. G., Yee, H. K. C., & Ellingson, E. 1997a, *ApJ*, 478, 462
- Carlberg, R.G., et al. 1997b, *ApJ*, 476, L7
- Carlberg, R.G., et al., 1997c, *ApJ* 485, L13
- Carlberg, R. G., Yee, H. K. C., Morris, S. L., Lin, H., Hall, P. B., Patton, D. R., Sawicki, M., & Shepherd, C. W. 2001, *ApJ*, 552, 427
- Clowe, D., Luppino, G. A., Kaiser, N., & Gioia, I. M. 2000, *ApJ*, 539, 540
- Clowe, D., & Schneider, P. 2001, *A&A*, 379, 384
- Colless, M., & Dunn, A.M. 1996, *ApJ*, 458, 435
- Colless, M., et al. 2001, *MNRAS*, 328, 1039
- Crone M. M., Evrard A. E., Richstone D. O., 1994, *ApJ*, 434, 402
- Dahle, H., Hannestad, S., & Sommer-Larsen, J. 2003, *ApJ*, 588, L73
- De Grandi, S., & Molendi, S. 2002, *ApJ*, 567, 163
- den Hartog, R., & Katgert, P. 1996, *MNRAS*, 279, 349

- de Theije, P. A. M., & Katgert, P. 1999, *A&A*, 341, 371 (paper VI)
- de Theije, P. A. M., Katgert, P., & van Kampen, E., 1995, *MNRAS*, 273, 30
- Diaferio, A. 1999, *MNRAS*, 309, 610
- Diaferio, A., & Geller, M. J. 1997, *ApJ*, 481, 633
- Dressler, A. 1980, *ApJ*, 236, 351
- Dupke, R. A., & Bregman, J. N. 2001, *ApJ*, 547, 705
- Ellingson, E., Lin, H., Yee, H. K. C., & Carlberg, R. G. 2001, *ApJ*, 547, 609
- Ettori, S., De Grandi, S., & Molendi, S. 2002, *A&A*, 391, 841
- Ettori, S., & Lombardi, M. 2003, *A&A*, 398, L5
- Ettori, S., Tozzi, P., & Rosati, P. 2003, *A&A*, 398, 879
- Firmani, C., D’Onghia, E., Avila-Reese, V., Chincarini, G., & Hernández, X. 2000, *MNRAS*, 315, L29
- Fischer, P., & Tyson, J. A. 1997, *AJ*, 114, 14
- Gebhardt, K., Pryor, C., Williams, T. B., Hesser, J. E. 1994, *AJ*, 107, 2067
- Geller, M. J., Diaferio, A., & Kurtz, M. J. 1999, *ApJ*, 517, L23
- Ghigna, S., Moore, B., Governato, F., Lake, G., Quinn, T., & Stadel, J. 1998, *MNRAS*, 300, 146
- Girardi, M., & Mezzetti M. 2001, *ApJ*, 548, 78
- Governato, F., Ghigna, S., Moore, B., Quinn, T., Stadel, J., & Lake, G. 2001, *ApJ*, 547, 555
- Heisler, J., Tremaine, S., & Bahcall, J. N. 1985, *ApJ*, 298, 8
- Hoekstra, H., Franx, M., Kuijken, K., & van Dokkum, P. G. 2002, *MNRAS*, 333, 911
- Hughes J. P., 1989, *ApJ*, 337, 21
- Irwin, J. A., & Bregman, J. N. 2000, *ApJ*, 538, 543
- Irwin, J. A., Bregman, J. N., & Evrard, A. E., 1999, *ApJ*, 519, 518
- Jing, Y. P., Mo, H. J., Börner, G., Fang, L. Z. 1995, *MNRAS*, 276, 417
- Jing, Y. & Suto, Y. 2000, *ApJ*, 529, L69
- Katgert, P., Mazure, A., den Hartog, R., Adami, C., Biviano, A., & Perea, J. 1998, *A&AS*, 129, 399 (paper V)

- Katgert, P., et al. 1996, *A&A*, 310, 8 (paper I)
- Kelson, D. D., Zabludoff, A. I., Williams, K. A., Trager, S. C., Mulchaey, J. S., & Bolte, M. 2002, *ApJ*, 576, 720
- Kent S. M., & Gunn J. E., 1982, *AJ*, 87, 945
- Kikuchi, K., Furusho, T., Ezawa, H. Yamasaki, N. Y., Ohashi, T., Fukazawa, Y., & Ikebe, Y. 1999, *PASJ*, 51, 301
- King, L. J., Clowe, D. I., Lidman, C., Schneider, P., Erben, T., Kneib, J.-P., & Meylan, G. 2002, *A&A*, 385, L5
- Lombardi, M., Rosati, P., Nonino, M., Girardi, M., Borgani, S., & Squires, G. 2000, *A&A*, 363, 401
- Mahdavi, A., Geller, M. J., Böhringer H., Kurtz, M. J., & Ramella, M., 1999, *ApJ*, 518, 69
- Mamon, G. 2000, in *ASP Conf. Ser. 197, Galaxy Dynamics: from the Early Universe to the Present*, ed. F. Combes, G.A. Mamon, & V. Charmandaris (San Francisco: ASP), 367
- Markevitch M., Forman W. R., Sarazin C. L., & Vikhlinin, A., 1998, *ApJ* 503, 77
- Markevitch, M., & Vikhlinin, A. 1997, *ApJ*, 491, 467
- Markevitch, M., Vikhlinin, A., Forman, W. R., & Sarazin, C. L. 1999, *ApJ*, 527, 545
- Melnick, J., & Sargent, W. L. W. 1977, *ApJ*, 215, 401
- Melott, A. L., Chambers, S. W., & Miller, C. J. 2001, *ApJ*, 559, L75
- Meneghetti, M., Yoshida, N., Bartelmann, M., Moscardini, L., Springel, V., Tormen, G., & White, S. D. M. 2001, *MNRAS*, 325, 435
- Merrifield, M. R., & Kent, S. M. 1989, *AJ*, 98, 351
- Merritt, D. 1987, *ApJ*, 313, 121
- Mohr, J. J., Geller, M. J., Fabricant, D. G., Wegner, G., Thorstensen, J., & Richstone, D. O. 1996, *ApJ*, 470, 724
- Moore, B., Quinn, T., Governato, F., Stadel, J., & Lake, G. 1999, *MNRAS*, 310, 1147 (M99)
- Natarajan, P., Kneib, J.-P., & Smail, I. 2002b, *ApJ*, 580, L11
- Natarajan, P., Loeb, A., Kneib, J.-P., & Smail, I. 2002a, *ApJ*, 580, L17
- Navarro, J. F., Frenk, C. S., & White, S. D. M. 1996, *ApJ*, 462, 536
- Navarro, J. F., Frenk, C. S., & White, S. D. M. 1997, *ApJ*, 490, 493 (NFW)

- Nevalainen, J., Markevitch, M., & Forman, W. 1999, *ApJ*, 526, 1
- Oemler, A. Jr. 1974, *ApJ*, 194, 1
- Plionis, M. 2002, *ApJ*, 572, L67
- Power, C., Navarro, J. F., Jenkins, A. et al. 2003, *MNRAS*, 398, 14
- Pratt, G. W., & Arnaud, M. 2002, *A&A*, 394, 375
- Reisenegger, A., Quintana, H., Carrasco, E. R., & Maze, J. 2000, *AJ*, 120, 523
- Ricotti, M. 2002, *MNRAS*, submitted (astro-ph/0212146)
- Rines, K., Geller, M. J., Diaferio, A., Mahdavi, A., Mohr, J. J., & Wegner, G. 2002, *AJ*, 124, 1266
- Rines, K., Geller, M. J., Diaferio, A., Mohr, J. J., & Wegner, G. A. 2000, *AJ*, 120, 2338
- Rines, K., Geller, M. J., Kurtz, M. J., Diaferio, A., Jarrett, T. H., & Huchra, J. P. 2001, *ApJ*, 561, L41
- Roettiger, K. & Flores, R. 2000, *ApJ*, 538, 92
- Sand, D. J., Treu, T., & Ellis, R. S. 2002, *ApJ*, 574, L129
- Schaeffer, R., Maurogordato, S., Cappi, A., & Bernardeau, F. 1993, *MNRAS*, 263, L21
- Shapiro, P. R., & Iliev, I. T. 2000, *ApJ*, 542, L1
- Smith, S. 1936, *ApJ*, 83, 23
- Solanes, J.M., & Salvador-Solé, E. 1990, *A&A*, 234, 93
- Squires, G., Kaiser, N., Fahlman, G., Babul, A., & Woods, D. 1996, *ApJ*, 469, 73
- Suginohara T., & Ostriker J.P., 1998, *ApJ*, 507, 16
- Takahashi, K., Sensui, T., Funato, Y., & Makino, J. 2002, *PASJ*, 54, 5
- Taylor, A. N., Dye, S., Broadhurst, T. J., Benitez, N., & van Kampen, E. 1998, *ApJ*, 501, 539
- Tamura, T., Makishima, K., Fukazawa, Y., Ikebe, Y., & Xu, H. 2000, *ApJ*, 535, 602
- The, L. S., & White, S. D. M. 1986, *AJ*, 92, 1248
- Thomas, T. 2003, in preparation (paper VIII)
- Thomas, T., Hartendorp, M., & Katgert, P. 2003, in preparation (paper IX)
- Thomas, T. & Katgert, P. 2003, in preparation (paper X)

- Thomas, P. A., Muanwong, O., Pearce, F. R., Couchman, H. M. P., Edge, A. C., Jenkins, A., & Onuora, L. 2001, MNRAS, 324, 450
- Tyson, J. A., Wenk, R. A., & Valdes, F. 1990, ApJ, 349, L1
- van der Marel, R. 1994, MNRAS, 270, 271
- van der Marel, R., Magorrian, J., Carlberg, R., Yee, H., & Ellingson, E. 2000, AJ, 119, 2038
- van Kampen, E., 1994, PhD thesis, Leiden University
- van Kampen, E., 1995, MNRAS, 273, 295
- Wallin, J. F., Yentis, D., MacGillivray, H. T., Bauer, S. B., & Wong, C. S. 1994, BAAS, 26, 897
- West, M. J., & Bothun, G. D. 1990, ApJ, 350, 36
- Yagi, M., Kashikawa, N., Sekiguchi, M., Doi, M., Yasuda, N., Shimasaku, K., & Okamura, S. 2002, AJ, 123, 87
- Zwicky, F. 1933, *Helv. Phys. Acta*, 6, 10
- Zwicky, F. 1937, ApJ, 86, 217